Design Considerations and Experimental Analysis of High-Voltage SiC Schottky Barrier Rectifiers

Kipp Jay Schoen, Jerry M. Woodall, *Fellow, IEEE*, James A. Cooper, Jr., *Fellow, IEEE*, and Michael R. Melloch, *Senior Member, IEEE*

***Abstract*— Practical design of high-voltage SiC Schottky rectifiers requires an understanding of the device physics that affect the key performance parameters. Forward characteristics of SiC Schottky rectifiers follow thermionic emission theory and are relatively well understood. However, the reverse characteristics are not well understood and have not been experimentally investigated in-depth. In this paper we report the analysis and experimental results of both the forward and reverse characteristics of high-voltage SiC Schottky rectifiers. Ti and Ni Schottky rectifiers with boron implant edge termination were fabricated on n-type 4H SiC samples. Ni Schottky rectifiers fabricated on a 13-μm thick 3.5×10^{15} cm^{-3} nitrogen doped epilayer have a current density of 100 A/cm^2 at approximately 2 V forward bias and a reverse leakage current density of less than 0.1 A/cm^2 at a reverse bias of 1720 V. The reverse leakage current is observed to depend on device area, Schottky barrier height, electric field at the metal-semiconductor interface, and temperature (a decreasing temperature dependence with increasing reverse bias). In addition, the reverse leakage current magnitude is larger and the electric field dependence is stronger than predicted by thermionic emission and image-force barrier height lowering. This suggests the reverse leakage current is due to a combination of thermionic field emission and field emission.**

***Index Terms*— High voltage, reverse leakage current, silicon carbide, Schottky barrier rectifiers.**

I. Introduction

LARGE bandgap semiconductors have been widely investigated and utilized for optoelectronic applications. However, research and commercial interest in large bandgap semiconductor and SiC electrical devices has recently increased due to the availability of high-quality SiC and general advances in material fabrication techniques. SiC is a promising power semiconductor because of its large bandgap (3.0 eV for 6H and 3.2 eV for 4H) and thermal conductivity (4.9 W/cmK for 6H and 4H) [1]. For power applications, SiC's large bandgap translates into a high critical field. A high critical electric field allows device designs that have lower series resistance and lower power dissipation. SiC power devices have been analyzed and shown to have substantial advantages when compared to Si and GaAs power devices [2]–[4].

In general, Schottky rectifiers are of interest because they are majority carrier devices and consequently have very fast switching times and no reverse recovery current. Si Schottky rectifiers are severely limited by the low critical field of Si and a relatively small range of possible barrier heights [5]. GaAs Schottky diodes are limited by the critical field of GaAs and Schottky barrier height pinning [5]. The relatively low barrier heights of Si and GaAs metal-semiconductor contacts lead to a substantial increase in reverse leakage current with increasing temperature. SiC Schottky rectifiers have been shown to have a strong dependence of metal-semiconductor barrier height on metal work function [6]. Therefore, Si and GaAs Schottky diodes dissipate more power and are limited to a smaller temperature range than comparable SiC Schottky diodes.

The SiC Schottky rectifier is a potentially important commercial device because it offers substantial performance benefits over Si and GaAs Schottky rectifiers and it is a relatively simple device to fabricate. The superior materials characteristics of SiC allow for the use of Schottky rectifiers in situations where Si and GaAs Schottky rectifiers are not practical. High-performance GaAs Schottky rectifiers with a forward current of up to 20 A and blocking voltages of up to 250 V are currently being used in applications such as electric motor drives and high-efficiency DC–DC converters [7]. It has also been shown that certain markets are willing to pay a premium for the improved device performance of GaAs Schottky rectifiers [8]. These issues make the SiC Schottky rectifier an excellent candidate for commercialization.

II. Theory and Analysis of Power Schottky Rectifiers

The optimal design of high-performance SiC Schottky rectifiers requires an understanding of the dominant device mechanisms that affect power Schottky rectifier performance. The key performance parameters of power Schottky rectifiers are breakdown voltage, forward voltage drop, reverse leakage current, power dissipation, and switching time. Depending on the application, different parameters become more or less important relative to others.

Each of these performance parameters are affected by one or more physical mechanism. Therefore, it is important to relate the key performance parameters to the device physics of Schottky contact rectifiers. In addition, SiC Schottky rectifier analysis requires the consideration of issues such as the effect of a large electric field at the metal-semiconductor interface. The typical Schottky rectifier consists of a metal contact deposited on an epilayer, a substrate, and a backside ohmic contact. The main device design variables that affect power Schottky rectifier characteristics are the contact metal

Manuscript received April 8, 1997; revised January 15, 1998. The review of this paper was arranged by Editor M. A. Shibib. This work was supported by the Office of Naval Research under Grant N00014-95-1-1302.

The authors are with the School of Electrical and Computer Engineering, Purdue University, West Lafayette, IN 47907 USA.

Publisher Item Identifier S 0018-9383(98)04606-1.

workfunction, the epilayer doping, the epilayer thickness, and the device edge termination.

A. Breakdown Voltage

The breakdown voltage of a Schottky rectifier depends on the semiconductor critical field, epilayer doping, epilayer thickness, and device edge termination. Therefore, the breakdown voltage may be used to determine the optimal epilayer doping and thickness under parallel plane avalanche breakdown conditions. The desired epilayer doping is the maximum doping that will sustain the specified breakdown voltage. The relationship for the epilayer doping is [9]

$$N_D = \frac{\varepsilon_s E_{CR}^2}{2qV_B} \tag{1}$$

where N_D is the epilayer doping, ε_S is the semiconductor dielectric constant, E_{CR} is the semiconductor critical field, q is the electron charge, and V_B is the breakdown voltage.

The corresponding epilayer thickness is the reverse bias depletion width at the breakdown voltage. The relationship between minimum epilayer thickness, the critical field, and the breakdown voltage is [9]

$$t_{\rm epi} = \frac{2V_B}{E_{CR}} \tag{2}$$

where $t_{\rm epi}$ is the minimum epilayer thickness.

Edge termination of devices is necessary to achieve the parallel plane breakdown voltage of a Schottky rectifier. Two-dimensional and three-dimensional field crowding of nonedge terminated devices increase the electric field at the contact edge well above the parallel plane electric field. MEDICI simulations show that the enhanced electric field can be more than twice the parallel plane electric field. Many edge termination techniques have been reported for SiC power devices including a field plate overlapping an oxide region [10], floating metal rings [11], p-type guard rings [12], highly resistive surface regions formed by argon implant [13]–[15], highly resistive surface regions formed by boron implant [16], and highly resistive regions formed by porous SiC [17]. Several of these techniques have been shown to sufficiently mitigate field crowding such that parallel plane breakdown voltages may be achieved.

B. Forward Voltage Drop

The forward voltage drop is a function of the Schottky barrier height and the series resistance. The forward voltage drop is [9]

$$V_F = \frac{nkT}{q}\ln\left(\frac{J_F}{A^*T^2}\right) + n\phi_B + R_{\rm ON}J_F \tag{3}$$

where V_F is the forward voltage drop, n is the ideality factor, k is Boltzman's constant, T is the temperature, J_F is the forward current density, A^* is the Richardson's constant, ϕ_B is the Schottky barrier height, and $R_{\rm ON}$ is the series or on-resistance.

The device on-resistance is a function of the epilayer doping and the epilayer thickness (neglecting the substrate and ohmic contact resistance). The on-resistance for a specified breakdown voltage is [9]

$$R_{\rm ON} \approx \rho_{\rm epi}t_{\rm epi} = \frac{t_{\rm epi}}{q\mu_n N_D} = \frac{4V_B^2}{\mu_n\varepsilon_s E_{CR}^3} \tag{4}$$

where $\rho_{\rm epi}$ is the epilayer resistivity, and μ_n is the epilayer mobility.

For an optimal device design, once the forward current density has been specified, and the required breakdown voltage has been used to determine the epilayer doping and thickness, the only remaining variable that affects the forward voltage drop is the Schottky barrier height. In general the forward voltage drop of experimental SiC Schottky rectifiers has agreed well with thermionic emission theory and devices with ideality factors near one and specific on-resistance near the theoretical minimum have been reported [6], [18]–[21].

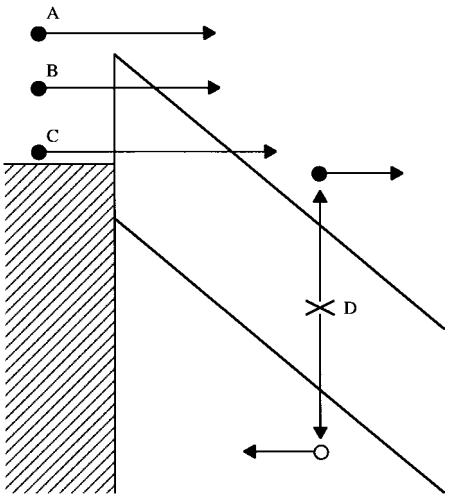

Fig. 1. Reverse bias current transport mechanisms of metal-semiconductor contacts: (a) thermionic emission, (b) thermionic field emission, (c) field emission, and (d) generation in the depletion region.

C. Reverse Leakage Current

The basic reverse leakage current mechanisms of a Schottky rectifier are shown in Fig. 1. The reverse leakage current mechanisms of a Schottky rectifier are (a) thermionic emission, (b) thermionic field emission, (c) field emission, and (d) generation in the depletion region [22]. In addition to these basic mechanisms, surface leakage and defect related leakage may occur. Real world devices likely contain current caused by more than one of these mechanisms. The dominant mechanism depends on the Schottky barrier height, temperature, and applied bias.

Thermionic emission reverse leakage current density depends on the Schottky barrier height and the temperature. The relationship between reverse leakage current density and Schottky barrier height is [5]

$$\begin{aligned} J_L &= A^*T^2e^{(-\phi_B/kT)}[e^{(qV/nkT)} - 1] \\ &= J_S[e^{(qV/nkT)} - 1] \approx -J_S \end{aligned} \tag{5}$$

where J_L is the reverse leakage current density, and J_S is the reverse saturation current density.

Thermionic emission reverse leakage current is also affected by image-force barrier height lowering. Image-force barrier height lowering decreases the effective Schottky barrier height by an amount that depends on the electric field at the metal-semiconductor interface. The image-force barrier height lowering is [5]

$$\Delta\phi_B = \sqrt{\frac{qE_M}{4\pi\varepsilon_s}} \tag{6}$$

where $\Delta\phi_B$ is the image-force barrier height lowering, and E_M is the electric field at the metal-semiconductor interface.

The thermionic emission reverse leakage current density, accounting for image-force barrier height lowering may be written as

$$J_L \approx -A^*T^2e^{(-\phi_B/kT)}e^{(\Delta\phi_B/kT)} = -J_Se^{(\Delta\phi_B/kT)}. \tag{7}$$

Experimentally, the reverse leakage current of both 6H and 4H SiC Schottky rectifiers have a larger magnitude than expected by thermionic emission and a stronger voltage dependence than predicted by image-force barrier height lowering [23]; reverse leakage current mechanisms other than thermionic emission must be considered. Thermionic field emission and field emission are typically not considered to contribute to the reverse leakage current of moderately and lightly doped Si Schottky rectifiers. However, the large critical field of SiC increases the likelihood of substantial thermionic field emission and field emission in SiC Schottky rectifiers. The magnitude and voltage dependence for the thermionic field emission and field emission of SiC Schottky rectifiers has been calculated and compared with experimental SiC Schottky rectifier reverse leakage currents [24]. These calculations agree relatively well with the experimental data and suggest that thermionic field emission and field emission must be considered as significant.

Both thermionic field emission and field emission are tunneling mechanisms that depend on the barrier height and width. The difference between thermionic field emission and field emission is that thermionic field emission is the tunneling of electrons thermally excited above the Fermi level of the metal while field emission is the tunneling of electrons at the Fermi level of the metal. Hence, thermionic field emission will depend on temperature and field emission will be independent of temperature.

The metal-semiconductor tunneling barrier may be approximated as a triangular barrier as shown in Fig. 2. The probability of tunneling through the triangular barrier depends on the zero bias Schottky barrier height, the image-force barrier lowering, and the electric field at the metal-semiconductor interface (which determines the barrier width since the slope of the triangular potential barrier is the electric field).

The relationship between tunneling current density and electric field for a triangular barrier may be expressed in terms of the electric field and the Schottky barrier height [22]

$$J_L \propto E_M^2e^{(-8\pi\sqrt{2m^*}\phi_B^{3/2}/3hqE_M)} \tag{8}$$

where m^* is the electron effective mass, and h is Planck's constant. The relationship between electric field and tunneling current density may be demonstrated by plotting

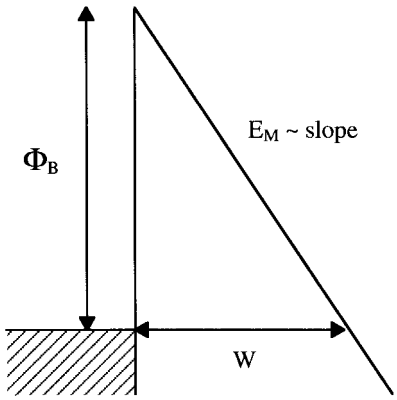

Fig. 2. Triangular barrier approximation and dimensions for a metal-semiconductor contact barrier.

(Fowler–Nordheim (FN) plot)

$$\ln(J_L/E_M^2) \propto 1/E_M. \tag{9}$$

Reverse leakage current caused by generation in the depletion region depends on the width of the depletion region. The relationship for depletion region generation reverse leakage current is [22]

$$J = \frac{qn_iW}{2\tau_r} \tag{10}$$

where n_i is the intrinsic carrier concentration, W is the width of the depletion region, and τ_r is the lifetime within the depletion region. The large bandgap of SiC makes n_i very small and virtually eliminates the likelihood of substantial depletion region generation reverse leakage current. Regardless of the dominant reverse leakage current mechanism, since the specified breakdown voltage determines the epilayer doping and thickness, the only remaining variable that significantly affects the reverse leakage current is the Schottky barrier height.

D. Power Dissipation

The power dissipation of a Schottky rectifier is dependent on the forward voltage drop and the reverse leakage current density. The power dissipation of a Schottky rectifier is [9]

$$P_D = (\%_{\rm ON})(V_FJ_F) + (1-\%_{\rm ON})(V_BJ_L) \tag{11}$$

where P_D is the power dissipated, and $\%_{\rm ON}$ is the on duty-cycle.

With respect to power dissipation, there is a tradeoff in selecting the best metal for a power Schottky rectifier. A metal that forms a small barrier will reduce the forward voltage drop but increase the reverse leakage current. Conversely, a metal that forms a large barrier will increase the forward voltage drop and decrease the reverse leakage current. It is important to consider the duty cycle, required forward current, and required breakdown voltage before selecting the Schottky contact metal.

E. Switching Time

The switching speed of a Schottky rectifier depends on the dominant forward current mechanism. Typical SiC Schottky devices are dominated by thermionic field emission and

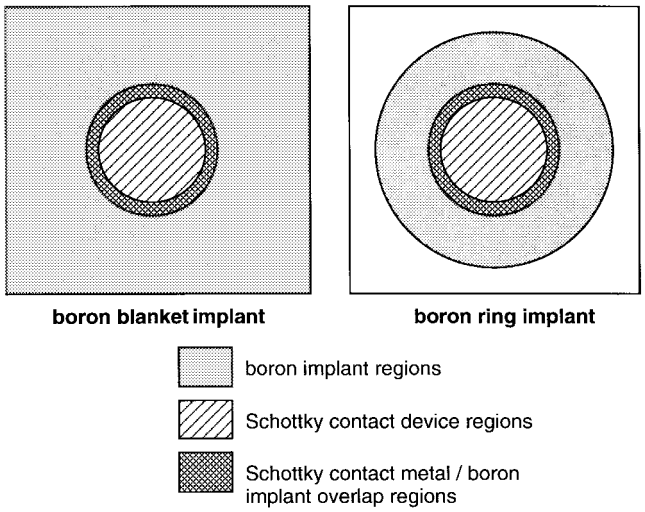

Fig. 3. Device structure of boron blanket implant and boron ring implant edge terminated 4H SiC high-voltage Schottky rectifiers.

consequently should have fast switching times compared to typical P-N and P-i-N rectifiers. Nonterminated platinum 6H SiC Schottky rectifiers have been shown to have turn-off times comparable to high-speed Si P-i-N rectifiers and no reverse recovery current [19].

III. Experimental Procedure

Two different n-type 4H Si-face SiC samples were used to fabricate both Ti and Ni Schottky rectifiers. The first sample has an epilayer doping of 3.5×10^{15} cm^{-3} and a thickness of 13 μm. The second sample has an epilayer doping of 1.6×10^{16} cm^{-3} and a thickness of 10 μm. Both samples have heavily doped n-type substrates. The material used in these experiments was acquired from Cree Research, Inc. Two samples of different epilayer doping and thickness were used to eliminate possible sample specific variations from the analysis.

A. Device Fabrication

Schottky rectifiers with boron implant edge termination were fabricated on both the 13- and 10-μm samples. Boron implant edge termination was selected for use because it has been shown to effectively suppress field crowding while not causing a significant increase in reverse leakage current [16]. Devices with both a blanket implant (implanting the entire surface except the active area of the device) and a 100-μm wide ring implant (implanting only a ring around the device) were fabricated. The basic device structure for the blanket implant devices and the ring implant devices is shown in Fig. 3. Both the blanket implant and the ring implant devices have a Schottky metal/implant region overlap of 20 μm.

Prior to implanting the boron edge termination, approximately 600 nm of Au was deposited and patterned for an implant mask. Next, a 1×10^{15} cm^{-2} dose of boron with an energy of 30 keV was used to implant the samples. After implantation, the Au implant mask was removed and the samples were annealed at 1050 °C for 90 min to remove implant lattice damage. The samples were then cleaned in piranha followed by a buffered oxide etch immediately prior to the Schottky contact metal deposition. Circular contacts of either Ti or Ni were deposited by ebeam evaporation and patterned by liftoff. The contacts range in size from 100 to 1200 μm diameter. Unannealed large area backside contacts were formed by thermally evaporating aluminum onto the unpolished heavily doped substrate.

B. Device Testing

Forward and reverse current–voltage (I–V) characteristics were measured for the Ti and Ni Schottky rectifiers. Device I–V characteristics were measured by directly probing individual Schottky rectifiers. The probe arms were configured with a single probe contacting the device top and a single probe contacting the backside ohmic contact. Devices were tested in an air ambient (no Fluroinert). The forward I–V characteristics were measured using an HP 4145 parameter analyzer. Reverse I–V characteristics were measured using a high-voltage test system. The high-voltage test system consists of a computer controlled high-voltage power supply (HVPS) (Stanford Research Systems PS350) and digital multimeter (Fluke 8840A). The HVPS is connected in series with the device under test and a resistor. The digital multimeter is used to measure the voltage across the resistor. The voltage applied to the device is determined by the output of the HVPS less the voltage drop across the resistor and the device current is determined from the voltage across the resistor. Forward and reverse I–V characteristics were measured at 20, 122, and 255 °C using a heated stage.

IV. Experimental Results

A. Measured Forward Characteristics

The forward I–V characteristics at 20, 122, and 255 °C for Ti and Ni Schottky contacts to the 10-μm sample are given in Fig. 4. The Ti and Ni Schottky contacts show near-ideal diode characteristics. The devices show an increase of reverse saturation current with increasing temperature, which is expected for devices dominated by thermionic emission. The extracted ϕ_{Bn} and ideality factors for the contacts at 20, 122, and 255 °C are given in Table I.

Both the Ti and the Ni contacts have approximately eight decades of linearity on a logarithmic plot at 20 °C and eventually roll-off because of device on-resistance. The on-resistance shows an increasing trend with increasing temperature. This is in accordance with reported Schottky rectifier on-resistance temperature dependencies. On-resistance temperature dependencies of $T^{1.6}$, $T^{2.0}$, and $T^{2.4}$ have been reported [18]–[21]. The forward I–V characteristics for Ti and Ni contacts to the 13-μm sample were measured at 20 °C and show results that are nearly identical to the 10-μm sample, with the exception of an earlier roll-off caused by a larger on-resistance, which is in accordance with the thicker, more lightly doped epilayer.

B. Measured Reverse Characteristics

The reverse I–V characteristics at 20 °C for Ni and Ti contacts to the 13-μm sample are given in Fig. 5. The Ni devices have a breakdown voltage of approximately 1720 V

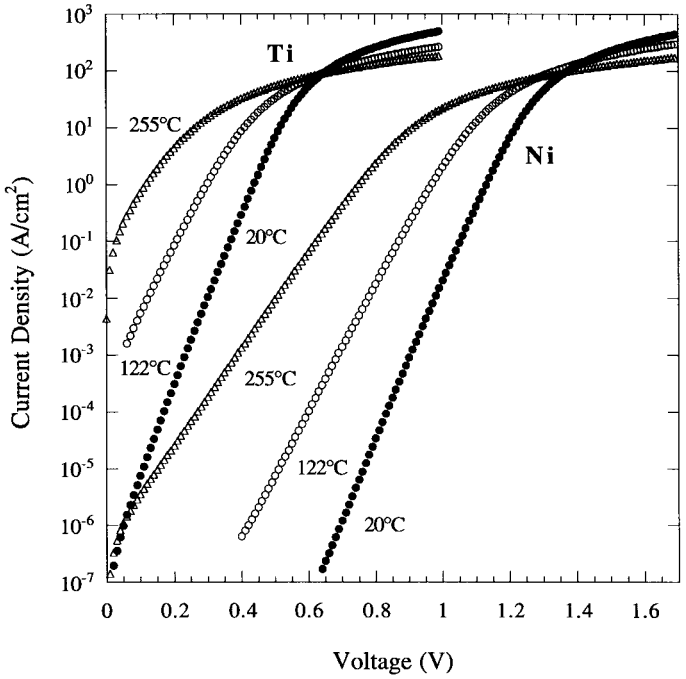

Fig. 4. Forward current–voltage characteristics at 20, 122, and 255 °C of Ti and Ni Schottky rectifiers on 1.6×10^{16} cm^{-3} doped 10 μm thick n-type Si-face 4H SiC.

TABLE I
MEASURED BARRIER HEIGHTS AND IDEALITY FACTORS AT 20, 122, AND 255 °C OF Ti AND Ni SCHOTTKY BARRIER RECTIFIERS ON n-TYPE Si-FACE 4H SiC. SiC EPILAYER DOPING IS 1.6×10^{16} cm^{-3} AND THICKNESS IS 10 μm

Metal	20°C		122°C		255°C	
	ϕ_{Bn}	n	ϕ_{Bn}	n	ϕ_{Bn}	n
Ti	0.80	1.15	0.85	1.10	N/A	N/A
Ni	1.3	1.21	1.4	1.12	1.5	1.12

and a reverse leakage current of less than 0.1 A/cm^2 at this voltage. The Ti devices show a larger reverse leakage current, which is in accordance with the smaller barrier height of the Ti contacts.

The reverse I–V characteristics at 20, 122, and 255 °C for Ti and Ni Schottky contacts to the 10-μm sample are given in Fig. 6. The Ti and Ni contacts show a reverse leakage current that increases with increasing temperature and increases with decreasing barrier height. The reverse I–V characteristics show a stronger reverse leakage current temperature dependence at low voltages than at high voltages. The Ti contacts' reverse leakage current and temperature dependence is comparable to reported reverse leakage current and temperature dependencies of high-voltage 4H SiC Ti Schottky rectifiers [16].

V. ANALYSIS OF RESULTS

A. Breakdown Voltage/Maximum Parallel Plane Electric Field

The critical field of a semiconductor increases with increased doping concentration caused by a corresponding increase in ionized impurity scattering and the consequent reduction in carrier scattering length. A measure of the effectiveness

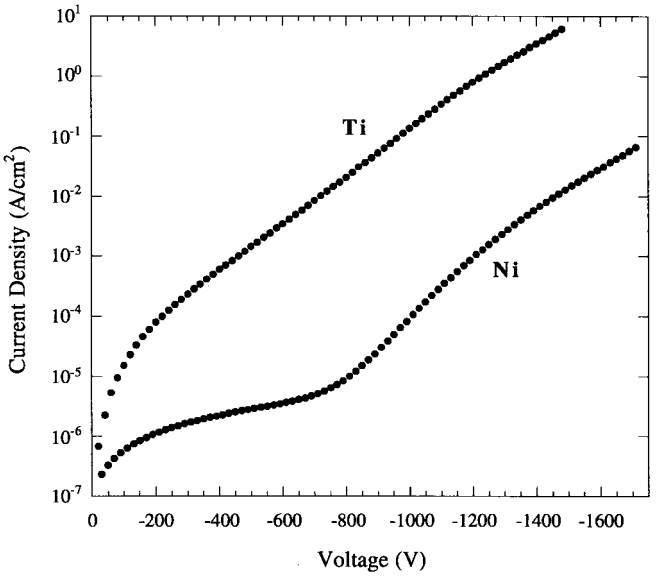

Fig. 5. Reverse current–voltage characteristics at 20 °C of Ti and Ni Schottky rectifiers on 3.5×10^{15} cm^{-3} doped 13 μm thick n-type Si-face 4H SiC.

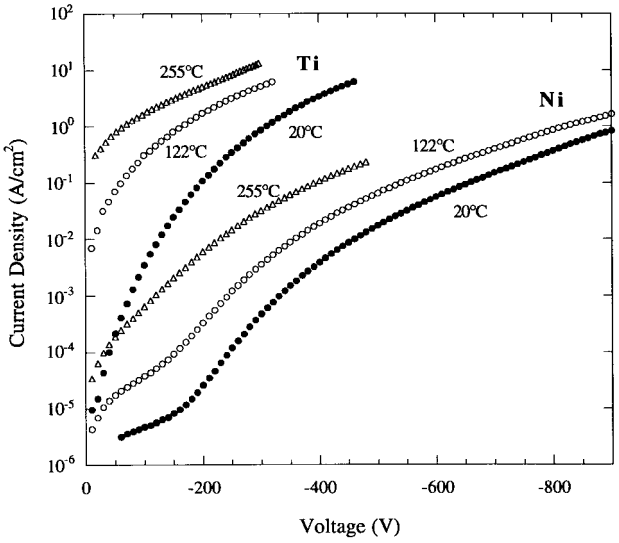

Fig. 6. Reverse current–voltage characteristics at 20, 122, and 255 °C of Ti and Ni Schottky rectifiers on 1.6×10^{16} cm^{-3} doped 10 μm thick n-type Si-face 4H SiC.

of device edge termination is the maximum parallel plane electric field achieved in a device. The maximum parallel plane electric field versus epilayer doping of reported 4H SiC mesa P-N rectifiers [25], non-punched-through 4H SiC Schottky rectifiers [16], punched-through 4H SiC Schottky rectifiers [16], and the 10- and 13-μm sample are given in Fig. 7. The relationship between the critical field of SiC and epilayer doping is estimated by fitting the measured mesa P-N rectifier data.

The maximum parallel plane electric fields obtained in the 10-μm sample (2.5 MV/cm) and the 13-μm sample (1.7 MV/cm) are in accordance with the fitted critical field doping relationship, indicating that the 10- and 13-μm sample devices are breaking down at or near the critical field. It has been suggested that punching through the epilayer may cause premature

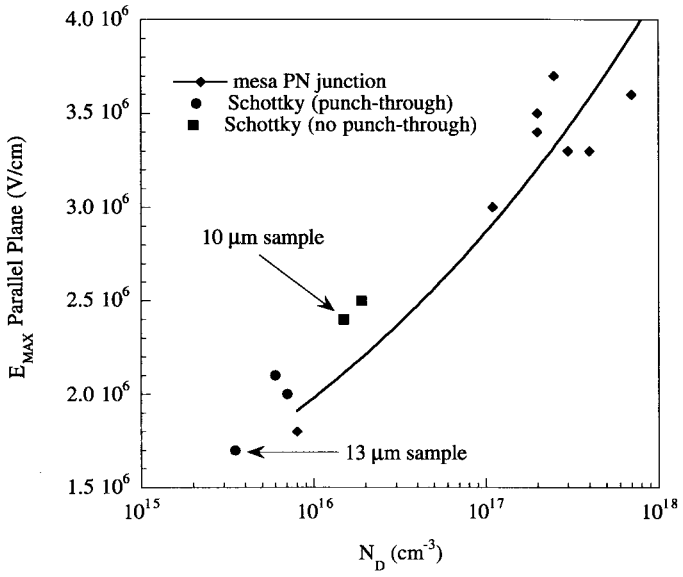

Fig. 7. Maximum parallel plane electric field versus epilayer doping for reported 4H SiC mesa P-N rectifiers, reported punched through 4H SiC Schottky rectifiers, reported non-punched-through 4H SiC Schottky rectifiers, and the 10- and 13-μm sample.

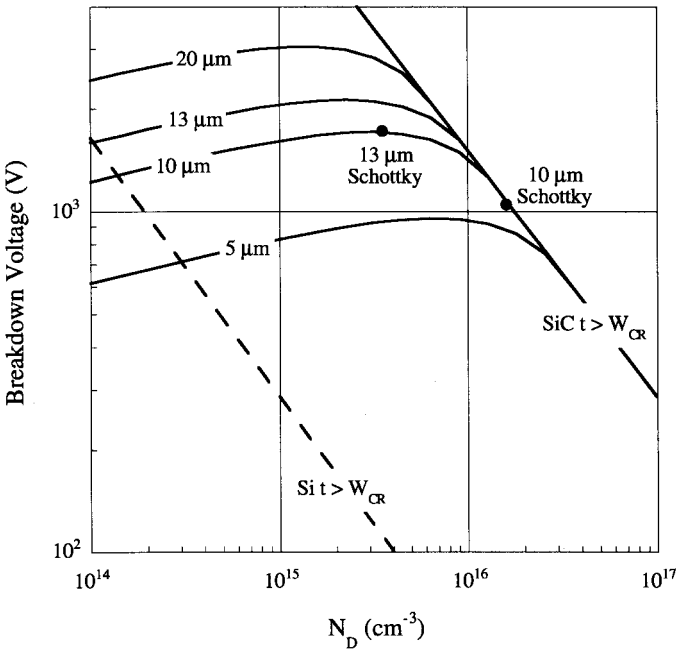

Fig. 8. Breakdown voltage versus epilayer doping of 4H SiC for punchthrough and non-punch-through epilayer thicknesses.

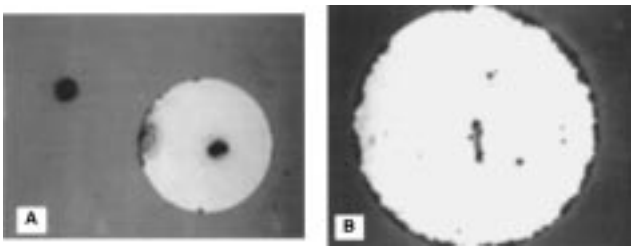

(a) (b)

Fig. 9. Device failure photos of: (a) blanket boron implant with a micropipe near the device causing a premature failure and (b) ring boron implant with uniform failure.

breakdown at less than the critical field. However, the data from the 13-μm sample (which is strongly punched through at breakdown) and the 10-μm sample (which is not punched through at breakdown) indicates that punchthrough does not cause premature breakdown. In addition, no significant "yield" differences (with respect to breakdown voltage) were observed between the strongly-punched-through and the non-punched-through devices.

A plot of breakdown voltage versus epilayer doping is given in Fig. 8. Since epilayer thickness is a practical constraint for lightly doped epilayers, breakdown voltage versus epilayer doping for both punchthrough and non-punch-through epilayer thicknesses is shown. The breakdown voltage for the 3.5×10^{15} cm^{-3} doped 13-μm thick sample and the breakdown voltage of the 1.6×10^{16} cm^{-3} doped 10-μm thick sample are also given in Fig. 8. It should be noted that for a given epilayer thickness, a decrease in epilayer doping does not necessarily increase the breakdown voltage since the decrease in doping may correspondingly decrease the critical field.

Blanket and ring boron implant edge terminations were compared. Both blanket and ring implants effectively reduce field crowding. However, the ring terminated devices showed a slightly higher breakdown voltage than the blanket terminated devices. The poorer performance of the blanket implant is likely caused by surface leakage to adjacent defects and a subsequent defect related failure. The ring implant confines the region of possible surface leakage. Consequently, if the main Schottky rectifier and ring regions are free of defects, the device will not suffer premature defect related breakdown.

Fig. 9 shows photographs of blanket and ring implant device failures. Photograph (A) is a device with boron blanket implant and shows a failure caused by surface leakage from the Schottky rectifier to a micropipe defect. Photograph (B) is a device with a boron ring implant and shows uniform failure around the edge of the device. The dark spots and scratches in the middle of the devices are from the probe tip being "welded" to the device during failure. The darkening of the device edges is due to the "burning" of the device edges during failure. These device failures were irreversible and resulted in destructive failure. Since the device failure is destructive, it is concluded that the failure mechanism is still related to field crowding at the device edge and is not due to avalanche breakdown under the main area of the device. However, devices that were reverse biased to near-breakdown voltages showed no signs of degradation when subjected to multiple voltage sweeps. Observed premature breakdown of devices was primarily attributable to micropipe defects and the device "yield" was therefore directly related to the material's micropipe density and device area (due to variations in material quality no attempt was made to quantify "yield").

B. Forward Voltage Drop

The measured specific on-resistance of the 13-μm sample is 5.6 mΩ cm^2 and the measured specific on-resistance of the 10-μm sample is 0.9 mΩ cm^2. The theoretical epilayer limited resistance of the 13-μm sample is 2.6 mΩ cm^2 and the theoretical epilayer resistance of the 10-μm sample is 0.4 mΩ cm^2.

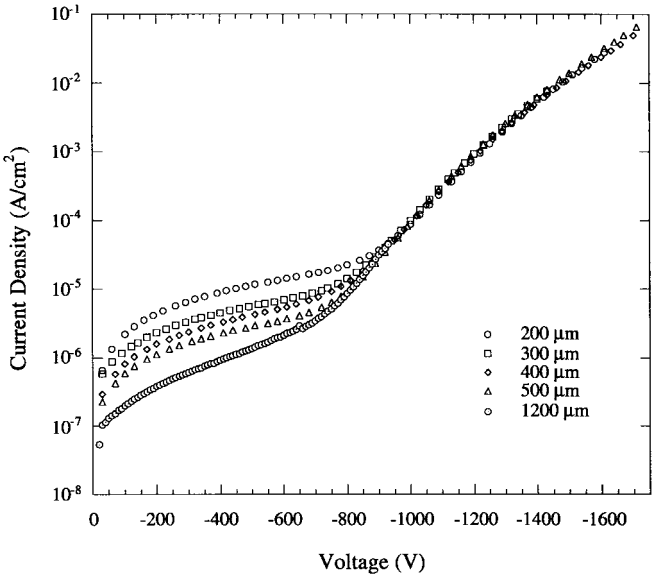

Fig. 10. Reverse current–voltage characteristics of Ni Schottky rectifiers on 3.5×10^{15} cm^{-3} doped 13-μm thick n-type Si-face 4H SiC for different size devices.

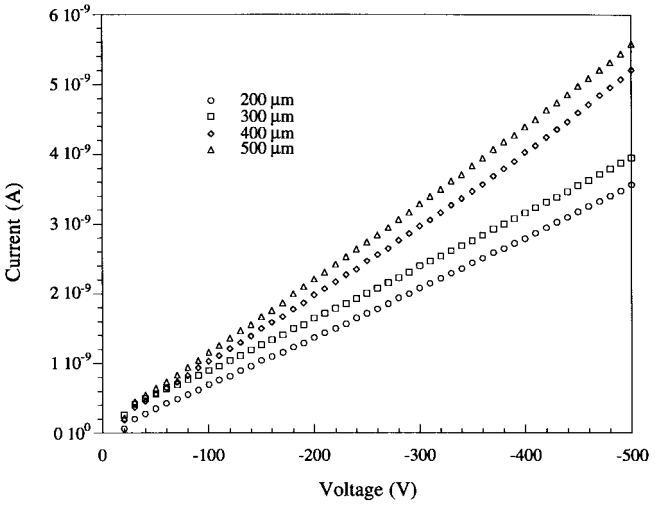

Fig. 11. 0 to 500 V reverse current–voltage characteristics of Ni Schottky rectifiers on 3.5×10^{15} cm^{-3} doped 13-μm thick n-type Si-face 4H SiC for different size devices.

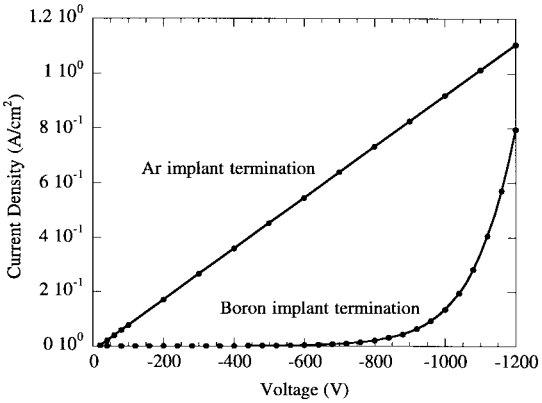

Fig. 12. Linear plot of reverse bias current density for reported argon implant edge terminated Schottky rectifiers and boron implant edge terminated Schottky rectifiers.

However, it should be noted that for low on-resistances (less than 1 mΩ cm^2) the substrate and ohmic contact contributions to the on-resistance are no longer negligible.

The forward bias I–V characteristic shown in Fig. 4 depicts the experimental dependence of the forward voltage drop on the metal-semiconductor barrier height. The temperature dependence of the forward voltage drop is also depicted in Fig. 4. While an increase in temperature increases the thermionic emission of the Schottky rectifier, it also increases the on-resistance. Therefore, for devices that operate in the on-resistance limited portion of the I–V characteristic, the forward voltage drop will increase with increasing temperature.

C. Reverse Leakage Current

A log plot of the current density versus voltage for different size Ni Schottky contacts to the 13-μm sample is given in Fig. 10. Fig. 10 shows that the reverse leakage current does not scale with device area at low reverse biases and does scale with device area at higher reverse biases. A linear I–V plot of four different size Ni Schottky rectifiers on the 13-μm sample for 0–500 V reverse bias is given in Fig. 11. This linearly related reverse leakage current is believed to be due to leakage through the highly resistive boron implanted edge termination regions. Since this reverse leakage current through the boron implanted region exhibits a linear I–V relationship, it may be thought of as a resistance in parallel to the Schottky rectifier (a shunt resistance). Previously tested nonterminated Ni Schottky rectifiers did not show this low bias reverse leakage current. This leakage through the boron implant regions is relatively small and is not evident for Ti Schottky rectifiers because the lower Schottky barrier height of Ti permits larger reverse leakage currents from other mechanisms. In addition, at higher reverse biases, reverse leakage mechanisms other than leakage through the boron implant region become dominant for the Ni Schottky rectifiers.

Highly resistive edge termination regions formed by argon implantation show a similar behavior, with a larger amount of leakage. In fact, devices terminated by argon implant regions exhibit a linear I–V relationship over the full range of reverse bias. A comparison of the reverse leakage of a boron implant terminated Ni Schottky contact to the 13-μm sample and published data [3] for argon implant terminated devices is given in Fig. 12. Fig. 12 shows that the argon implant terminated devices have a smaller shunt resistance than the boron implant terminated devices and consequently have reverse I–V characteristics that are dominated by the leakage through the argon implant regions.

Figs. 5 and 6 show that Ti and Ni boron edge terminated devices have a reverse leakage current that depends on Schottky barrier height. The 13-μm sample is punched through at 560 V reverse bias and the depletion width remains essentially constant for additional increases in reverse bias. Therefore, since the reverse leakage current depends on barrier height and is independent of depletion width, generation in the depletion region is not the dominant reverse leakage current mechanism.

Fig. 13 shows the reverse leakage current density versus the parallel plane electric field at the metal-semiconductor

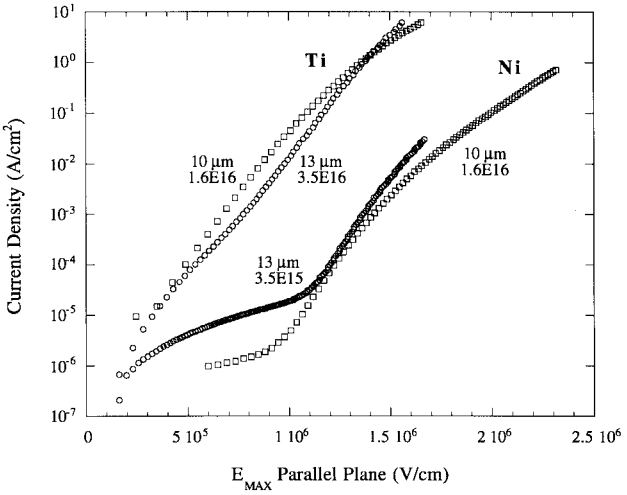

Fig. 13. Reverse bias current density at 20 °C versus electric field of Ti and Ni Schottky barrier rectifiers on both 3.5×10^{15} cm^{-3} doped 13-μm thick and 1.6×10^{16} cm^{-3} doped 10-μm thick n-type Si-face 4H SiC.

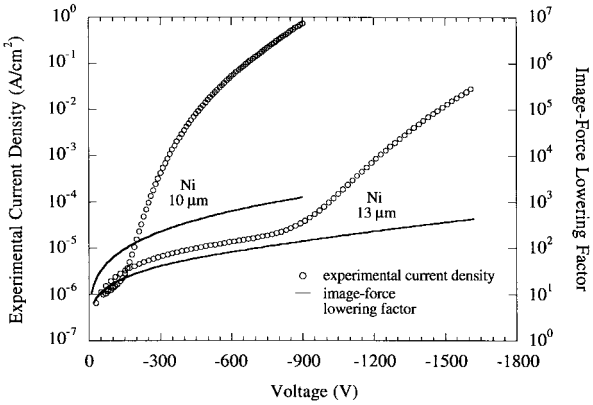

Fig. 14. Comparison of reverse bias current density and image-force multiplication factor for both 3.5×10^{15} cm^{-3} doped 13 μm thick and 1.6×10^{16} cm^{-3} doped 10 μm thick n-type Si-face 4H SiC.

interface for both the 13- and the 10-μm sample. The reverse leakage current is shown to depend on the barrier height and the electric field at the metal-semiconductor interface. While the reverse leakage current of the 10-μm sample is greater than the reverse leakage current of the 13-μm sample for a given reverse bias, the reverse leakage currents for both samples are essentially the same when plotted versus electric field at the metal-semiconductor interface. Therefore, reverse leakage current is shown to be sample and doping independent.

The theoretical increase in current density caused by image-force lowering and the experimental current density are plotted in Fig. 14 for both the 10- and the 13-μm sample. Fig. 14 shows that the maximum increase of thermionic emission reverse leakage current for either sample is three orders of magnitude or less while the increase in experimental reverse leakage current density for both samples is greater than five orders of magnitude. The magnitude of the reverse leakage current density predicted by thermionic emission is much less than the magnitude of the experimental reverse leakage current density. Therefore, thermionic emission reverse leakage current is not the dominant reverse leakage current mechanism.

Schottky rectifier reverse bias thermionic field emission and field emission depend on the tunneling barrier height and

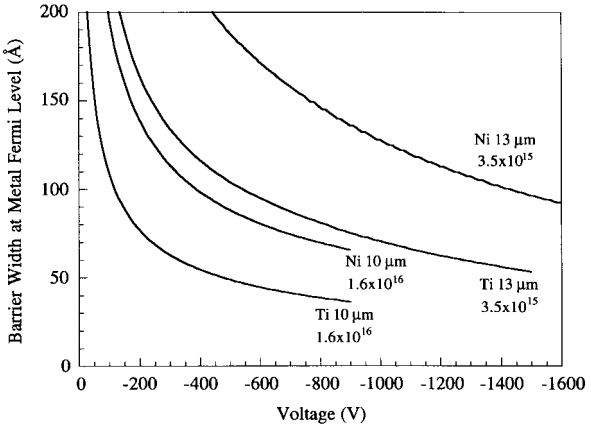

Fig. 15. Triangular barrier width versus reverse bias for both 3.5×10^{15} cm^{-3} doped 13 μm thick and 1.6×10^{16} cm^{-3} doped 10 μm thick n-type Si-face 4H SiC.

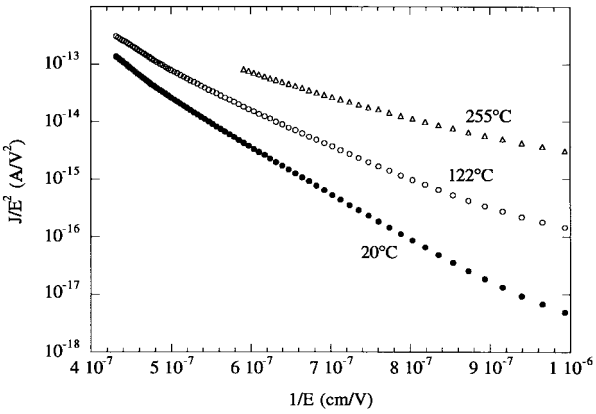

Fig. 16. FN plot of Ni Schottky contact on 1.6×10^{16} cm^{-3} doped 10-μm thick epilayer sample at 20, 122, and 255 °C.

width. Using the triangular barrier approximation given in Fig. 2, Ti and Ni Schottky barrier widths for the 10- and the 13-μm sample as a function of reverse bias were calculated and are plotted in Fig. 15. Since tunneling can become significant for barriers on the order of 10 nm wide, tunneling is a possible reverse leakage mechanism in these devices.

A temperature dependent plot of the relationship between tunneling current density and electric field given in (9) for Ni Schottky rectifiers on the 10-μm sample is shown in Fig. 16 (FN plot). Fig. 16 shows an increase of reverse leakage current density with increasing temperature. Fig. 16 also shows a stronger temperature dependence at low electric fields than at large electric fields suggesting that the reverse leakage current is comprised of both thermionic field emission and field emission. At small electric fields, the reverse leakage current appears to be dominated by thermionic field emission while at large electric fields field emission becomes more significant. Therefore, the dominant reverse leakage current mechanism is believed to be a combination of thermionic field emission and field emission.

A numerical calculation of the total tunneling current from thermionic field emission and field emission for a Schottky barrier with a barrier height of 1.1 eV and a doping of 3.6×10^{16} cm^{-3} has previously been done [24]. This cal-

TABLE II
SUMMARY OF 13-μm SAMPLE AND 10-μm SAMPLE EXPERIMENTAL PARAMETERS, RESULTS, AND OBSERVATIONS

13 μm Sample			10 μm Sample		
device parameter		value	**device parameter**		value
epilayer doping (cm^{-3})		3.5×10^{15}	epilayer doping (cm^{-3})		1.6×10^{16}
epilayer thickness (μm)		13	epilayer thickness (μm)		10
measurements			**measurements**		
forward I-V at 20°C			forward I-V at 20°C, 122°C, and 255°C		
reverse I-V at 20°C			reverse I-V at 20°C, 122°C, and 255°C		
results			**results**		
breakdown voltage (V)		1720	breakdown voltage (V)		1050
maximum electric field (V/cm)		1.7×10^{6}	maximum electric field (V/cm)		2.5×10^{6}
on-resistance ($m\Omega\ cm^2$)		5.6	on-resistance ($m\Omega\ cm^2$)		0.9
	Ti	Ni		Ti	Ni
20°C ϕ_B (eV)	0.85	1.5	20°C ϕ_B (eV)	0.80	1.3
20°C n	1.1	1.1	20°C n	1.2	1.2
Observations					
forward current is due to thermionic emission					
reverse leakage current depends on:					
1. device area					
2. barrier height					
3. electric field					
4. temperature					

culation shows a reverse leakage current increase of about five orders of magnitude for an increase of electric field from 8.2×10^{5} V/cm to 2.3×10^{6} V/cm. In addition, the calculation was performed for 300K and 373K, and shows a decreasing temperature dependence with increasing electric field.

VI. SUMMARY AND CONCLUSIONS

High-voltage Ti and Ni Schottky rectifiers with a highly resistive boron implant edge termination have been fabricated and tested. A summary of the experiment and results are given in Table II. Reverse breakdown shows near-ideal parallel plane breakdown. Forward characteristics are near-ideal and show an increasing on-resistance with increasing temperature. Reverse characteristics show a reverse leakage current that depends on device area, Schottky barrier height, electric field at the metal-semiconductor interface, and temperature. The reverse leakage current is larger than predicted by thermionic field emission and image-force barrier lowering and is believed to be a combination of thermionic field emission and field emission.

REFERENCES

[1] P. G. Neudeck, "Progress in silicon carbide semiconductor electronics technology," *J. Electron. Mater.*, vol. 24, p. 283, 1995.
[2] M. Bhatnager and B. J. Baliga, "Comparison of 6H-SiC, 3C-SiC, and Si for power devices," *IEEE Trans. Electron Devices*, vol. 40, pp. 645–655, Mar. 1993.
[3] C. E. Weitzel, J. W. Palmour, C. H. Carter, Jr., K. Moore, K. J. Nordquist, S. Allen, C. Thero, and M. Bhatnagar, "Silicon carbide high-power devices," *IEEE Trans. Electron Devices*, vol. 43, pp. 1732–1741, Oct. 1996.
[4] B. J. Baliga, "Trends in power semiconductor devices," *IEEE Trans. Electron Devices*, vol. 43, pp. 1717–1731, Oct. 1996.
[5] S. M. Sze, *Physics of Semiconductor Devices.* New York: Wiley, 1981.
[6] A. Itoh, O. Takemura, T. Kimoto, and H. Matsunami, "Barrier height analysis of metal/4H-SiC Schottky contacts," in *6th SiC Rel. Mater. Conf. Proc.*, 1995, pp. 685–688.
[7] Motorola Power Semiconductor Products rectifier application notes.
[8] R. A. Metzger and M. Meyer, "Rectifiers: A new application for GaAs," *Compound Semicond.*, pp. 12–15, July/Aug. 1996.
[9] B. J. Baliga, *Power Semiconductor Devices.* Boston, MA: PWS, 1996.
[10] J. N. Su and A. J. Steckl, "Fabrication of high-voltage SiC Schottky barrier diodes by Ni metallization," in *Proc. 1995 Conf. Silicon Carbide and Rel. Mater.*, pp. 697–700.
[11] M. Bhatnagar, H. Nakanishi, S. Bothra, P. K. McLarty, and B. J. Baliga, "Edge terminations for SiC high-voltage Schottky rectifiers," in *5th Int. Symp. Power Semiconductor Devices and IC's*, 1993, pp. 89–94.
[12] K. Ueno, T. Urushidani, K. Hashimoto, and Y. Seki, "The guard-ring termination for the high-voltage SiC Schottky barrier diodes," *IEEE Electron Device Lett.*, vol. 16, pp. 331–332, July 1995.
[13] D. Alok, B. J. Baliga, and P. K. McLarty, "A simple edge termination for silicon carbide devices with nearly ideal breakdown voltage," *IEEE Electron Device Lett.*, vol. 15, pp. 394–395, Oct. 1995.
[14] D. Alok, B. J. Baliga, M. Kothandaraman, and P. K. McLarty, "Argon implanted SiC device edge termination: Modeling, analysis, and experimental results," in *6th SiC Rel. Mater. Conf. Proc.*, 1995, pp. 565–568.
[15] D. Alok, R. Raghunathan, and B. J. Baliga, "Planar edge termination for 4H-silicon carbide devices," *IEEE Trans. Electron Devices*, vol. 43, pp. 1315–1317, Aug. 1996.
[16] A. Itoh, T. Kimoto, and H. Matsunami, "Excellent reverse blocking characteristics of high-voltage 4H-SiC Schottky rectifiers with boron-implanted edge termination," *IEEE Electron Device Lett.*, vol. 17, pp. 139–141, Mar. 1996.
[17] C. I. Harris, A. O. Konstantinov, C. Hallin, and E. Janzén, "SiC power device passivation using porous SiC," *Appl. Phys. Lett.*, vol. 66, no. 12, pp. 1501–1502, Mar. 20, 1995.
[18] A. Itoh, T. Kimoto, and H. Matsunami, "High performance of high-voltage 4H-SiC Schottky barrier diodes," *IEEE Electron Device Lett.*, vol. 16, pp. 280–282, June 1995.
[19] M. Bhatnagar, P. K. McLarty, and B. J. Baliga, "Silicon-carbide high-voltage (400 V) Schottky barrier diodes," *IEEE Electron Devices*, vol. 13, pp. 501–503, Oct. 1992.
[20] T. Kimoto, T. Urushidani, S. Kobayashi, and H. Matsunami, "High-voltage (>1 kV) SiC Schottky barrier diodes with low on-resistances," *IEEE Electron Device Lett.*, vol. 14, pp. 548–550, Dec. 1993.
[21] R. Raghunathan, D. Alok, and B. J. Baliga, "High-voltage 4H-SiC Schottky barrier diodes," *IEEE Electron Device Lett.*, vol. 16, pp. 226–227, June 1995.
[22] E. H. Rhoderick and R. H. Williams, *Metal-Semiconductor Contacts*, 2nd ed. Oxford, U.K.: Clarendon, 1988.
[23] M. Bhatnagar, B. J. Baliga, H. R. Kirk, and G. A. Rozgonyi, "Effect of surface inhomogeneties on the electrical characteristics of SiC Schottky contacts," *IEEE Trans. Electron Devices*, vol. 43, pp. 150–156, Jan. 1996.
[24] J. Crofton and S. Sriram, "Reverse leakage current calculations for SiC Schottky contacts," to be published.
[25] J. W. Palmour, J. A. Edmond, H. S. Kong, and C. H. Carter, Jr., "Vertical power devices in silicon carbide," in *Proc. 1993 Int. Conf. SiC and Rel. Mater.*

Kipp Jay Schoen received the B.S. degree (magna cum laude) in electrical engineering from Kansas State University, Manhattan, in 1989. While at Kansas State, he received a Rotary International Scholarship for business management studies at the University of Kent at Canterbury, U.K. His studies at Canterbury included a bilingual exchange program with the University of Deusto in San Sebastián, Spain. In 1992, he received a Master of European Business Administration with distinction from Canterbury. In 1993, he enrolled in the electrical engineering solid state devices and physics Ph.D. program at Purdue University, West Lafayette, IN, where he worked on silicon carbide and compound semiconductor devices. His main area of focus was high-temperature and power Schottky rectifier device design, fabrication, characterization, and analysis. He received the Ph.D. degree in May 1997.

He worked as an Embedded Computer System Designer at the Johns Hopkins Applied Physics Laboratory, Baltimore, MD. While working at the Applied Physics Laboratory, he studied applied semiconductor physics received the M.S. degree in applied physics in 1992. Currently, he is a Semiconductor Technology Product Manager at Hewlett Packard, Fort Collins, CO.

Jerry M. Woodall (SM'84–F'90) received the B.S. degree in metallurgy in from the Massachuesetts Institute of Technology, Cambridge, in 1960.

In 1982, he pioneered the horizontal Bridgman growth of both high purity and highly perfect GaAs crystals, and the fabrication of SiC p-n junctions using both Al diffusion and the traveling solvent method. He then pioneered the development of the liquid phase epitaxial (LPE) growth of Si doped GaAs IR high efficiency LED's used today in remote control applications such as TV sets. This was followed by seminal work on the LPE growth of GaAlAs and GaAlAs/GaAs heterojunctions used in super-bright red LED's and lasers used, for example, in CD players and short link optical fiber communications. Currently, he is the Charles William Harrison Distinguished Professor of Microelectronics at Purdue University, West Lafayette, IN. His present work involves the MBE growth III–V materials and devices with special emphasis on metal contacts and doping studies. His efforts are recorded in more than 200 publications in the open literature, 62 issued U.S. patents, and 10 patent applications filed.

Mr. Woodall's accomplishments have been recognized by five major IBM Research Division Awards, 30 IBM Invention Achievement Awards, the 1980 Electronics Division Award of the Electrochemical Society, the 1984 IEEE Jack A. Morton Award, the 1985 State State Science and Technology Award of the Electrochemical Society, the 1988 Heinrich Welker Gold Medal, and the International GaAs Symposium Award, his election as Fellow of the Electrochemical Society in May of 1990, his election to the National Academy of Engineering in 1989, his election to Electrochemical Society Fellow in 1992, and American Vacuum Society Fellow in 1994; the 1990 Medard Welch (Founders) Award form the American Vacuum Society, and IBM Corporate Award in 1992 for the invention of the GaAlAs/GaAs heterojunction. He has been a member of AVS since 1981, and since has worked on behalf of AVS as EMPD Program Chair (1983), EMPD Division Chair (1984), National Meeting Program Chair (1985), and AVS Director (1986–1988, 1995–1997), AVS President-Elect (1996–1997). He is also the recipient of the Eta Kappa Nu Vladimir Karapetoff Eminent Members' Award for 1997.

James A. Cooper, Jr. (S'66–M'69–SM'85–F'93) received the B.S.E.E. degree from Mississippi State University, Starkville, in 1968, the M.S.E.E degree from Stanford University, Stanford, CA, in 1969, and the Ph.D. degree from Purdue University,West Lafayette, IN, in 1973.

He joined the Technical Staff of Bell Laboratories, Murray Hill, NJ, in August, 1973. While at Bell Labs, he served as Principal Designer on the WE-8000, AT&T's first CMOS microprocessor, and with D. F. Nelson, developed a time-of-flight technique for measuring the drift velocity of electrons in inversion layers of silicon. In August 1983, he became Professor of Electrical Engineering at Purdue University, where he was founding Director of the Purdue Optoelectronics Research Center. His current research is focused on wide bandgap semiconductors, with emphasis on microwave and power switching devices. He has coauthored more than 150 technical papers and conference presentations, four book chapters, and holds ten U.S. patents.

Prof. Cooper served as Associate Editor of IEEE TRANSACTIONS ON ELECTRON DEVICES from 1983 to 1986.

Michael R. Melloch (S'66–M'79–SM'97) received the B.S.E.E., M.S.E.E., and Ph.D. degrees from Purdue University, West Lafayette, IN, in 1975, 1976, and 1981, respectively.

From June 1976 to August 1978, he was a Design Engineer at Intel Corporation, where he worked on the 8275, a CRT controller chip; the 8748, the first single-chip microcomputer; and was co-designer of the 8051, a second-generation single-chip microcomputer. In February 1982, he joined the Central Research Laboratories at Texas Instruments as a member of the Technical Staff. At Texas Instruments his research interests centered around GaAs surface acoustic wave devices. In August 1984, he joined the School of Electrical Engineering at Purdue University as an Assistant Professor and is presently a Full Professor there and former Assistant Dean of Engineering. He has coauthored 275 conference talks, 210 technical papers, two book chapters, and is holder of five U.S. patents. His group at Purdue University was the first to investigate the effect of bandgap narrow in GaAs—caused by heavy inpurity doping on the electrical performance of devices. They were also the first to characterize both the electron and hole minority carrier mobilities in GaAs as a function of majority carrier concentration using a zero-field time-of-flight technique. He has been involved with development of a nonvolatile memory cell in 6H-SiC, the development of the first digital integrated circuits and CCD's in SiC; the development of the first DMOS power transistor; and the characterization and improvement of SiO_2/SiC interface. He was involved with the discovery of arsenic clusters in GaAs epilayers that were grown at low substrate temperatures by MBE and subsequently annealed, and the development of many electrical and optical applications of these composite materials. In 1993, he co-founded MellWood Laboratories with Prof. Jerry Woodall and Dr. Eric Harmon. MellWood Laboratories is a supplier of custom epitaxy and high-speed photodectectors.

Dr. Melloch has served as a Symposium Co-Organizer of the 1993 Spring Meeting of the Material Research Society, the Program Chair for the 1994 North American Conference on Molecular Beam Epitaxy; Co-Organizer of the Eighth International Conference on Superlattices, Microstructures, and Microdevices; and Associate Program Chair for the 1997 International Symposium on Compound Semiconductors. In 1993, he was elected to the Electronics Materials Committee of TMS, and has served as Secretary (1995–1997) and Vice-Chair (1997–1999). He has been Guest Editor for five journal special issues. He is a Fellow of the American Physical Society, and a member the American Vacuum Society, the Minerals, Metal & Materials Society and the Optical Society of America.